Postprint of: Śliwiński P., The methodology of design of axial clearances compensation unit in hydraulic satellite displacement machine and their experimental verification, Archives of Civil and Mechanical Engineering, Vol. 19, iss. 4 (2019), pp. 1163-1182, DOI: 10.1016/j.acme.2019.04.003

The methodology of design of axial clearances compensation unit in hydraulic satellite displacement machine and their experimental verification

Pawel Sliwinski, Ph.D., D.Sc., Eng., *pawel.sliwinski@pg.edu.pl*
Gdansk University of Technology, Faculty of Mechanical Engineering

A new methodology of calculating the dimensions of the axial clearance compensation unit in the hydraulic satellite displacement machine is described in this paper. The methods of shaping the compensation unit were also proposed and described. These methods were used to calculate the geometrical dimensions of the compensation field in an innovative prototype of a satellite hydraulic motor. This motor is characterized by the fact that the body rotates. In other words, the planet (an inner element of the working mechanism) is stationary and the curvature (an external element of the working mechanism) is rotating. The inflow and outflow ports are located in the motor pin which replaces its shaft. The results of the analytical calculation of the compensation field geometrical dimensions were used in FEM calculations of the compensation plate deformation. The correctness of the design of axial clearance compensation unit has been verified experimentally. The experimental method consists in measuring leaks in the gaps of the working mechanism and measuring the torque at low constant speed of the motor case. The results of experimental test are also described in this paper. This way, it has been proven that the proposed new analytical methodology for the design of the axial clearance compensation unit in the hydraulic satellite displacement machine is correct.

Keywords: *compensation unit, satellite motor, hydraulic motor, axial clearances, satellite mechanism, advanced design*

1. Introduction

The hydraulic positive-displacement machines (a hydraulic motor and a pump) are the most important elements in the hydraulic system. The energy carrier in hydraulic systems is a liquid whose type is determined by the requirements for the system. Another type of liquid will be used in the hydraulic systems of a floating platform or in a mobile platform [1,2] and another type in the hydraulic control system of a turbine [3]. Mineral oil is the liquid that is commonly used in hydraulic systems. However, in some industrial sectors, a non-flammable (mining, steel mills, etc.) or non-toxic for the environment and human health (food industry) liquid is required. Especially water as a working liquid is increasingly used in hydraulic systems. Elements of such systems must be made of non-corrosive steel or coated with special coatings [4,5].

The type of liquid influences energy conversion in the hydraulic positive-displacement machines. Both the pump and the hydraulic motor are components of the hydraulic system in which there are energy losses, such as volumetric, mechanical and pressure. Volumetric losses in the working mechanism of a displacement machine can be reduced by maintaining or reducing the size of the gaps under pressure. However, this requires the development and use of a special structural unit in the displacement machine. This unit is called the clearance compensation unit of working mechanism elements or, briefly, the clearances compensation unit. Two types of compensation units are known in the realm of hydraulic displacement machines: compensation of axial clearances and compensation of radial clearances [6,7,8,9,10,11,12].

It should be noted that there is no universal method for designing positive displacement machines with compensation units. Every type of hydraulic device requires a separate design approach. In some cases the basic design methods are used but in other cases, new design methods are sought. For example, in [13] was described methodology which allows careful planning and

systematic execution so that the whole design task reduces to a logical and comprehensible exercise and also allows recovery from inevitable errors. The same process was used in the design of the hydraulic engine described in this article. But in [14] was shown that viscoelastic elements (like rubber-like components) used in machine design can be incorporated in machine analysis, just as in the case of conventional elements (e.g. gears, cogs, chain drives, bearings). This is achieved by introducing elementary theory and models, by describing new and established experimental techniques for determining viscoelastic properties, and finally, by working through actual examples. In power hydraulics, viscoelastic elements are rarely used. In this way, the theory of viscoelastic elements is not used in the design of hydraulic motors. Plastics are more and more often used for the construction of positive displacement machines, of course. An example can be a hydraulic cylinder with plastic components [15] and the gerotor pump where the working mechanism was built of polyoxymethylene [16].

In the research and development of the construction of positive displacement machines, advanced numerical calculations are used also. For example in [17] the deformation of the piston guide and rear/front sliding bearings of a hydraulic motor in a deep-sea environment is analyzed in detail using the Ansys software. Of course, numerical methods are used to analyze phenomena occurring in displacement machines. For example, in [18] the leakage past the tooth flanks of the gears in transition contacts in involute external toothed gear pump is analyzed in details using CFD in Fluent-Ansys software. But in [7,19] are described the strength calculations of an element compensating circumferential backlash in the external toothed gear pump taking into account the minimum values of the height of the gaps. Such an analysis in effect allows the constructors to draw conclusions as to the selection of the size of the gaps in the gear pump. Similar considerations regarding the size of the gaps in the axial piston pump are described in [20,21]. Furthermore, in this publications, the pressure distribution in oil film and the hydrostatic load of the valve plate-cylinder block system in an axial piston pump were analysed. The R&D problems concern not only the positive displacement machines. In valves are also the design problems, that scientists are working on. For example, in [22] the author focuses on the vibrations description of the slide–sleeve pair of a hydraulic distributor.

A separate issue is the phenomena occurring in hydraulic machines working in low ambient temperature. It has been shown that in machines with high volumetric efficiency, they may be damaged as a result of the loss of axial clearances of moving parts [23,24].

It should be noted that there is also no general method for designing a clearance compensation unit that is suitable for different types of positive-displacement machines. Each type of hydraulic displacement machine requires an individual method of designing the clearance compensation unit [8,9,10,11,12,25]. Such an individual approach is required for satellite displacement machines. The design of these machines has already been described, among others, in [26,27,28,29]. The immediate spark for the development of the design methodology of the axial clearance compensation unit in satellite machines started with designing an innovative hydraulics satellite motor with a rotating body [30,31,32]. The design of this motor is described in this paper. This motor can be used, for example, in auxiliary systems for truck wheels drive, in belt conveyor drives, in winding machines drives, etc.

Therefore, the development of a new method of the design of the compensation unit in a satellite displacement machine is a new, appropriate and justified issue. Consequently, the following objectives have been defined for this paper:

a) description of known methods of designing of an axial compensation unit;
b) formulation of the method, that is:
   - analysis of pressure fields and forces acting on the commutation plates in a classic satellite machine (rotating shaft) and in a satellite machine with a rotating body,
   - formation of the axial clearance compensation unit in satellite machines and calculation of the geometrical dimensions of the compensation pressure field;

c) using an example – satellite motor with axial clearance compensation unit;
d) verification, that is:
   – FEM calculations of compensation plates deformation in the motor and verification of geometrical dimensions of the compensation pressure field,
   – experimental verification of the correct operation of the compensation unit in a prototype of the motor.

2. Axial clearance compensation in positive-displacement machines

When the differential pressure increases in the positive-displacement machine, the deformation of the working mechanism elements K also increases (Fig. 1a). There is an increase of axial clearances Δh_{ARE} and Δh_{BRE} between the working mechanism elements resulting in a leakage increase. This is an undesirable effect that can be counteracted by using an axial clearances compensation unit CP. The task of this compensation unit is to reduce the axial clearance Δh_{ARE} and Δh_{BRE} of the moving elements of the working mechanism (Fig. 1b). In this way leakages in the mechanism are limited and, consequently, the volumetric efficiency of the displacement machine is improved.

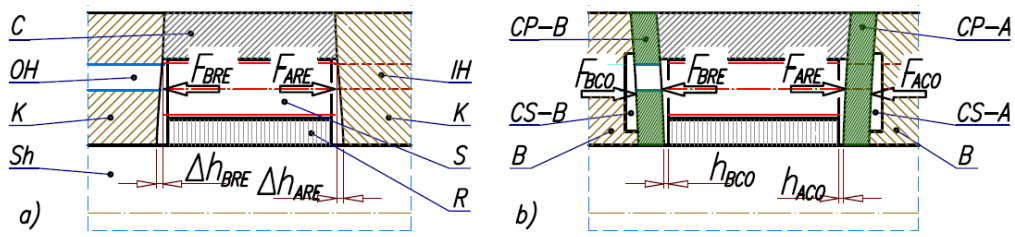

Fig. 1. Axial clearances of working mechanism elements in loaded positive-displacement machine: a) without a compensation unit – clearances Δh_{ARE} and Δh_{BRE}; b) with compensation unit – clearances Δh_{ACO} and Δh_{BCO}; F_{ARE} and F_{BRE} – repulsive forces (forces from the pressure in the working chamber); F_{ACO} and F_{BCO} – compensation forces (forces from the pressure in the compensation space CS-A and CS-B respectively); R, S and C – elements of working mechanism; B – body (case) or manifold; OH and IH – outflow and inflow channels; CP-A and CP-B – compensation elements (plates)

An axial clearance compensation unit is used in rotary positive-displacement machines such as: satellite pumps and motors, gear pumps and motors, orbital pumps and motors and vane pumps. The differences between particular construction designs of a compensation unit consist mainly in a different shape and configuration of the compensation field.

In the literary sources, only general principles about the design of an axial clearance compensation unit are given. These principles are simple cases of compensation units in a gear pump, gear motor or orbital pump and motor [2,6,8,9,10]. In these machines, an additional component (or components) limiting the axial clearances of the working mechanism element is used (Fig. 1b).

According to [8], two conditions must be met in order to ensure correct operation of the axial clearance compensation unit:
a) the compensation force F_{CO} (a force pushing a compensation element) must be greater than a repulsive force F_{RE}:

$$F_{RE} \leq F_{CO} \tag{1}$$

b) the directions of forces F_{CO} and F_{RE} should be collinear.

Furthermore, according to K. Elgert [8], the value of compensation force F_{CO} can be changed by changing the value of the compensation field and the value of the compensation pressure.

The compensation force F_{CO} cannot take unlimited values. This force is limited by the size of the compensation field and by the tribological properties of the elements cooperating with each other. The force F_{CO} which has the appropriate value reduces the height of the gaps and thus

reduces the leakage. In this way, the volumetric efficiency of the machine is bigger. The force F_{CO} which has too high a value eliminates the axial clearances of working mechanism elements. Hence, there is no leakage and large friction forces develop. Thus, the mechanical efficiency of the machine decreases and, even, the working mechanism may suffer damage. Therefore, the value of force F_{CO} should be selected in such a way that the overall efficiency of the hydraulic positive-displacement machine is as high as possible [8].

In literary sources, the values of force F_{CO} are only given for gear pumps. The maximum value of this force is assumed as [8,9,10]:

$$F_{CO} = (1 \div 1{,}3) \cdot F_{RE} \tag{2}$$

The condition (1) and the condition (2) are insufficient because they can only be true if the repulsive force F_{RE} and the compensation force F_{CO} are collinear, or a distance between these forces is very small. Otherwise, the moment bending the compensation plate appears and the idea of axial clearances compensation is not preserved.

Furthermore, the existing descriptions of the design solutions for an axial clearance compensation unit, do not contain information about the values of stresses and deformations in compensation unit elements.

The new methodology of designing a compensation unit in satellite machines, described in details in next parts of this paper, is based on balancing two moments bending the compensation plates. The dimensions of the compensation field are determined from the equation of the moment equilibrium. The first bending moment is a moment of force repulsing a compensation plate, while the second is a moment of compensation force. The repulsive force is a force obtained from pressure in satellite mechanism and acting on the compensation plate. The compensation force, however, is generated by the pressure acting on a compensation field on the compensation plate on the other side of this plate. Thus, in order to correctly determine the compensation field in different types of satellite machines, the following sequence should be run:

1) choosing the appropriate configuration of compensation unit (as in Fig. 10 ÷ Fig. 15);
2) calculating the compensation field and their dimmensions;
3) creating a design of satellite machine;
4) performing the calculations of deformation and stress in the elements of a loaded satellite machine;
5) manufacturing a prototype of the satellite machine and experimental verification the correctness of the compensation operation.

3. Satellite working mechanisms and pressure distribution on the surface of commutation plates

The concept of the satellite machine working mechanism is based on the mutual cooperation of two non-round elements through circular gears (satellites S) between them. The rotor R has external teeth and the curvature C has internal teeth (Fig. 2). Satellites act as:

a) movable, tight barriers between HPC and LPC working chambers;
b) inflow and outflow distributors – as the working chamber passes from the filling phase to the extrusion phase (or vice versa), the satellites close or open the respective holes in the side plates (commutation plate) [26,27].

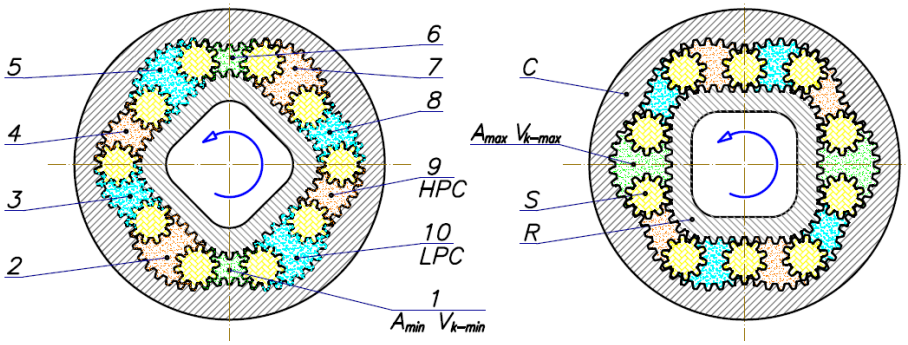

Fig. 2. Satellite mechanism of type II [31,32,33]: C – curvature, R – rotor, S – satellite, 1÷10 – working chambers, HPC – high pressure chambers (chamber with pressure p_{inH}), LPC – low pressure chambers (chamber with pressure p_{inL}), $V_{k\text{-}min}$ – working chamber with minimum volume (dead chamber) and with minimum area A_{min}, $V_{k\text{-}max}$ – working chamber with maximum volume and with maximum area A_{max}

The satellite mechanism can be used to build a positive-displacement machine, i.e. a pump or a motor. It is also possible to build a machine with a motionless curvature (that is a typical machine with the shaft) or with a motionless rotor (machine with a rotating body) (Fig. 3). In the first case there is an axial clearance of the rotor R (Fig. 3a) and in the second case there is an axial clearance of the curvature C (Fig. 3b). Thus, two gaps with a height h_A and h_B exist in both cases. Specifically, in the working mechanism with motionless curvature these gaps exist between rotor R and compensation plates CP-A and CP-B (Fig. 3a). Similarly, in the working mechanism with motionless rotor these gaps exist between curvature C and compensation plates CP-A and CP-B (Fig. 3b). Dimensions h_A and h_B are the heights of gaps in an unloaded satellite machine. In loaded machine leaks exist in these gaps – from working chambers HPC and LPC to the space of shaft (for the case of motionless curvature) or to the area of motor (or pump) body (for the case of motionless rotor).

The inflow holes IH in a commutation plate CP-A are connected with the high pressure working chambers HPC (pressure p_{inH}) but the outflow holes OH in a commutation plate CP-B are connected with the low pressure working chambers LPC (pressure p_{inL}) (Fig. 2 and Fig. 3).

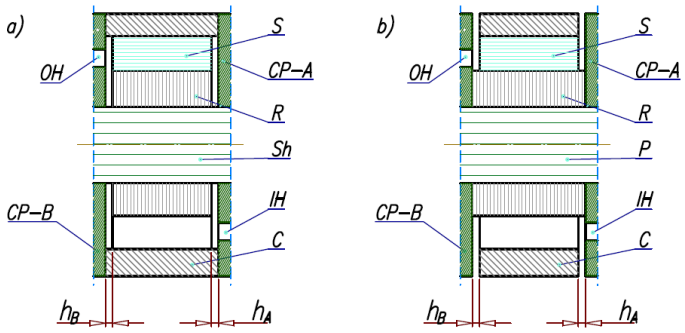

Fig. 3. Schematic drawing of satellite displacement machine: a) with a motionless curvature C; b) with a motionless rotor R; CP-A and CP-B – commutation (also compensation) plates, IH and OH – inflow and outflow channels, Sh – shaft, P – pin, S – satellite

These pressures in working chambers act on the commutation plates. The field of pressure on the commutation plate depends on:

a) an area of the working chamber which, in turn, depends on the rotor's (or curvature) rotation angle;
b) an area of the lateral surface of the satellite;
c) an area A_R of the lateral surface of the rotor (for a mechanism with motionless curvature) (Fig. 4);
d) an area A_C of the lateral surface of the curvature (for a mechanism with motionless rotor) (Fig. 6);

e) an area of inflow/outflow holes in commutation plates (Fig. 3).

Furthermore, additional pressure fields appear on the CP-A plate with inflow holes IH and others occur on the CP-B plate with outflow holes OH. For further analysis, it was assumed that:

a) the pressure in the gap between the commutation plate and satellite is the average pressure defined as:

$$p_{av} = \frac{p_{inH} + p_{inL}}{2} \tag{3}$$

b) the pressure in a chamber with maximum volume is average pressure p_{av};
c) the pressure in a dead chamber (chamber with minimum volume) is average pressure p_{av};
d) in the case of motionless curvature:
   – the pressure in the gap between the commutation plate and the rotor is average pressure p_{av};
   – there are no gaps, no liquid and no pressure on lateral surfaces of the curvature between the curvature and the commutation plate;
e) in the case of a motionless rotor (rotating curvature):
   – the pressure in the gap between the commutation plate and curvature is average pressure p_{av};
   – there are no gaps, no liquid and no pressure of liquid on lateral surfaces of the rotor between the rotor and the commutation plates.

Pressure fields on commutation plates for satellite mechanism with motionless curvature are shown in Fig. 4 and Fig. 5. The particular symbols on these figures are described in Tab. 1. It is necessary to notice that:

a) for different angle position of the rotor R the values of fields are different. For example, the value of H_{B1} from Fig. 4a is different from the value of H_{B1} from Fig. 4b or Fig. 4c;
b) for position of rotor R as in Fig. 4c and Fig. 5c there are no fields A_{max} and A_{min} with average pressure. High pressure fields H_{A3} and H_{B3} occur instead;
c) for rotor position corresponding to A_{max} and A_{min} (Fig. 4a, Fig. 4b, Fig. 5a and Fig. 5b) the amount of high pressure fields on the commutation plate CP-A is four, but on the commutation plate CP-B it is six.

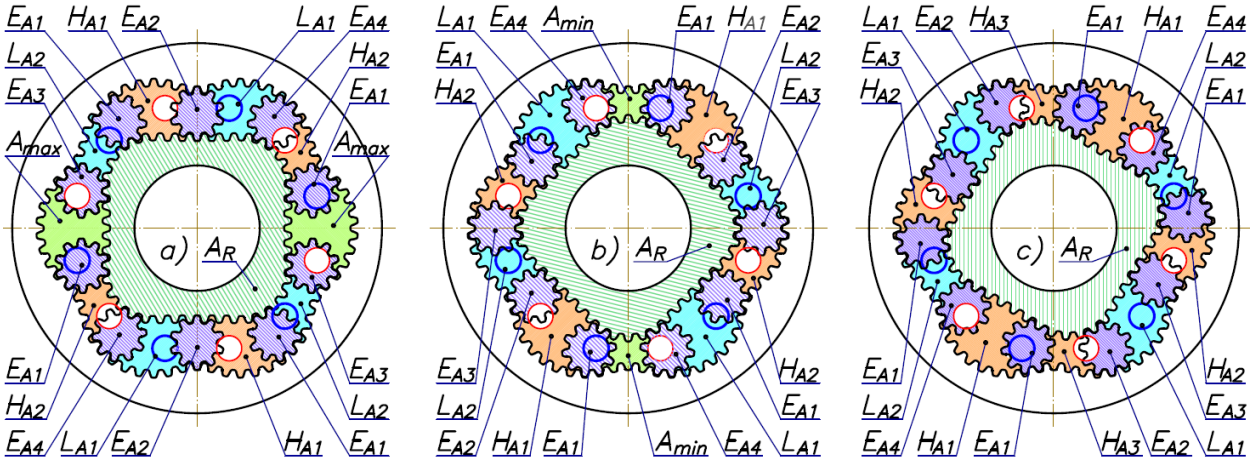

Fig. 4. Pressure fields on the commutation plate CP-A. Working mechanism with motionless curvature. The arrangement of the mechanism corresponding to: a) A_{max}; b) A_{min}; c) the largest possible values of fields H_{A1}. Symbols described in Tab. 1

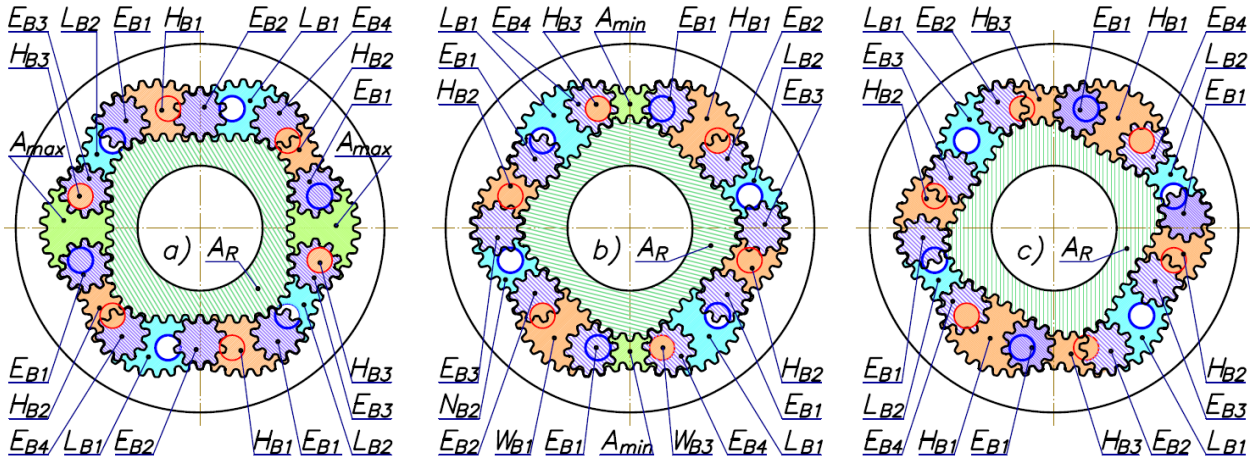

Fig. 5. Pressure fields on the commutation plate CP-B. Working mechanism with motionless curvature. The arrangement of the mechanism corresponding to: a) A_{max}; b) A_{min}; c) the largest possible values of fields H_{B1}. Symbols described in Tab. 1

Tab. 1. Symbols used in Fig. 4, Fig. 5, Fig. 6 and Fig. 7

H_{A1}, H_{A2} and H_{A3}	fields of high pressure on plate CP-A
H_{B1}, H_{B2} and H_{B3}	fields of high pressure on plate CP-B
L_{A1} and L_{A2}	fields of low pressure on plate CP-A
L_{B1} and L_{B2}	fields of low pressure on plate CP-B
E_{A1}, E_{A2}, E_{A3} and E_{A4}	fields of average pressure on plate CP-A
E_{B1}, E_{B2}, E_{B3} and E_{B4}	fields of average pressure on plate CP-B
A_{max}	field of chamber with maximum volume (field of average pressure)
A_{min}	field of chamber with minimum volume (field of average pressure)

The calculations of the value of the fields presented in the Fig. 4 and Fig. 5 performed with the analytical method are very difficult. It is much easier and recommended by the author to read them directly from the CAD documentation. It is recommended to read the value of fields for three positions of working mechanism as shown in Fig. 4 and Fig. 5.

Pressure fields on commutation plates in the satellite mechanism with a motionless rotor are shown in Fig. 6 and Fig. 7. In this case, A_C is the field of lateral surface of curvature (field of average pressure). The analysis of pressure fields is the same as for the satellite mechanism with motionless curvature.

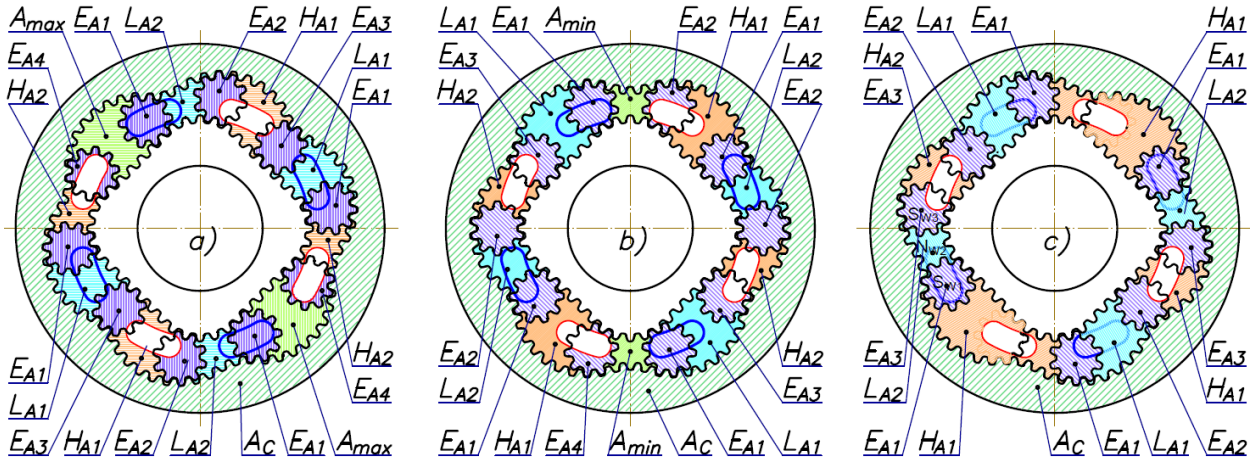

Fig. 6. Pressure fields on the commutation plate CP-A. Working mechanism with motionless rotor. The arrangement of the mechanism corresponding to: a) A_{max}; b) A_{min}; c) the largest possible values of fields H_{A1}. Symbols described in Tab. 1

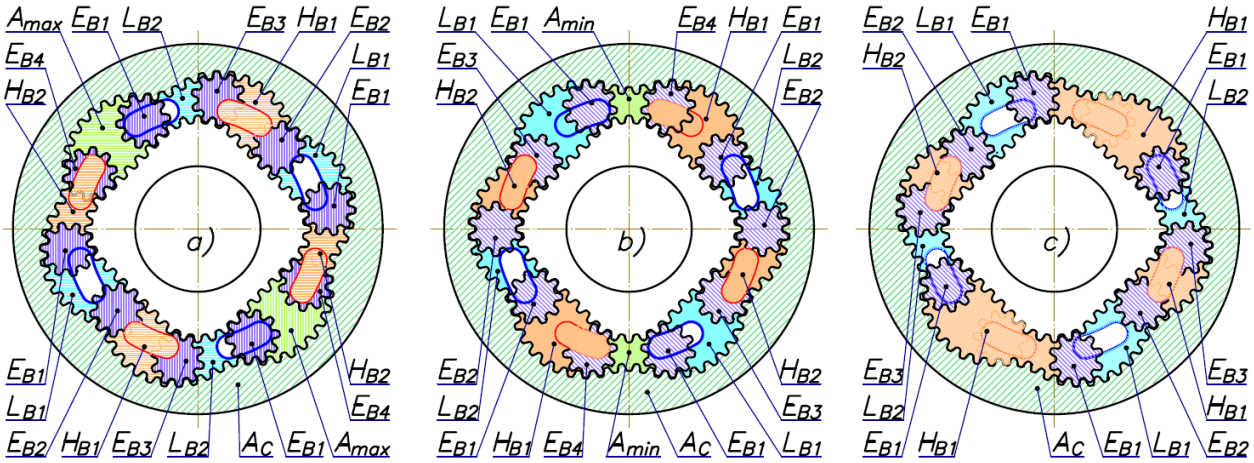

Fig. 7. Pressure fields on the commutation plate CP-B. Working mechanism with motionless rotor. The arrangement of the mechanism corresponding to: a) A_{max}; b) A_{min}; c) the largest possible values of fields H_{B1}. Symbols described in Tab. 1

4. Forces acting on the commutation plate

When pressures acting on the appropriate fields of commutation plates in working mechanism occur, forces that push these plates from the working mechanism are then created (Fig. 8).

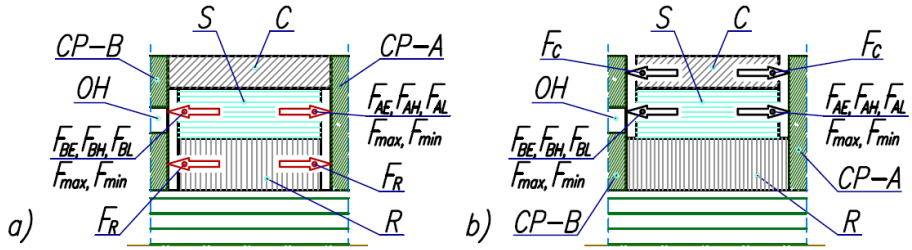

Fig. 8. Forces pushing commutation plates from the working mechanism: a) working mechanism with motionless curvature; b) working mechanism with motionless rotor. Symbols described in text

These forces are:

– F_R – the force resulting from average pressure p_{av} acting on the lateral surface A_R of the rotor:

$$F_R = A_R \cdot p_{av} \tag{4}$$

– F_C – the force resulting from average pressure p_{av} acting on the lateral surface A_C of the curvature:

$$F_C = A_C \cdot p_{av} \tag{5}$$

– F_{AEi} and F_{BEi} – forces resulting from average pressure p_{av} acting on the lateral surface E_{Ai} and E_{Bi} (index "i" means the number of fields as in Fig. 4) of satellites respectively:

$$F_{AEi} = E_{Ai} \cdot p_{av} \tag{6}$$

$$F_{BEi} = E_{Bi} \cdot p_{av} \tag{7}$$

– F_{AHi} and F_{BHi} – forces resulting from high pressure p_{inH} acting on the field H_{Ai} and H_{Bi} respectively:

$$F_{AHi} = H_{Ai} \cdot p_{inH} \tag{8}$$

$$F_{BHi} = H_{Bi} \cdot p_{inH} \tag{9}$$

– F_{ALi} and F_{BLi} – forces resulting from low pressure p_{inL} acting on the field L_{Ai} and L_{Bi} respectively:

$$F_{ALi} = L_{Ai} \cdot p_{inL} \tag{10}$$

$$F_{BLi} = L_{Bi} \cdot p_{inL} \tag{11}$$

– F_{Amax} – the force resulting from average pressure p_{av} acting on the field A_{max}:

$$F_{Amax} = 2 \cdot A_{max} \cdot p_{av} \tag{12}$$

– F_{Amin} – the force resulting from average pressure p_{av} acting on the field A_{min}:

$$F_{Amin} = 2 \cdot A_{min} \cdot p_{av} \tag{13}$$

Depending on the rotation angle of the rotor (or the curvature):

– $F_{Amax} = 0$ and $F_{Amin} = 0$ (for example as in Fig. 4a and Fig. 4b);
– $F_{Amax} = 0$ or $F_{Amin} = 0$ (for example as in Fig. 4c).

The resultant force F_{ARE} that repels the commutation plate CP-A from the satellite mechanism is:

$$F_{ARE} = F_R(F_C) + \sum_i^n F_{AEi} + \sum_i^n F_{AHi} + \sum_i^n F_{ALi} + F_{Amax} + F_{Amin} \tag{14}$$

Similarly, the resultant force F_{BRE} that repels the commutation plate CP-B from the satellite mechanism is:

$$F_{BRE} = F_R(F_C) + \sum_i^n F_{BEi} + \sum_i^n F_{BHi} + \sum_i^n F_{BLi} + F_{Amax} + F_{Amin} \tag{15}$$

Formulas (14) and (15) are true for the working mechanism with motionless curvature and motionless rotor. It is then necessary to use F_R or F_C instead $F_R(F_C)$ respectively.

The value F_{ARE} and F_{BRE} can be calculated from the following formula:

$$F_{ARE}(F_{BRE}) = \underbrace{A_{COH} \cdot p_{inH}}_{F_{REH}} + \underbrace{A_{COL} \cdot p_{inL}}_{F_{REL}} \tag{16}$$

where:

– A_{COH} – the theoretical field on the commutation plate corresponding to the high pressure working chambers;
– A_{COL} – the theoretical field on the commutation plate corresponding to the low pressure working chambers.

Fields A_{COH} and A_{COL} are calculated according to formula (25) which takes into account the fact that both high pressure and low pressure working chambers operate cyclically.

Regardless of the methods of calculating the resultant repulsive force described above, its value depends on the angle of rotor rotation (or depends on the angle of curvature rotation in the case of a satellite mechanism with motionless rotor).

As an effect of action of F_{ARE} and F_{BRE} forces we can observe:

a) deformation of commutation plates with the values Δh_{ARE} and Δh_{BRE} (Fig. 9);
b) shift with the values x_{ARE} and x_{BRE} (Fig. 9) (that is, loss of contact) of motionless elements:
   – for a mechanism with motionless curvature – the commutation plates with the curvature,
   – for a mechanism with motionless rotor – the commutation plates with the rotor.

The effect of a commutation plate deformation is:

a) for a mechanism with a motionless curvature – an increase of axial clearance between satellites and rotor;
b) for a mechanism with a motionless rotor – an increase of axial clearance between satellites and curvature.

The increase of the axial clearance is:

$$\Delta h_{RE} = \Delta h_{ARE} + \Delta h_{BRE} + x_{ARE} + x_{BRE} \tag{17}$$

As a consequence, in a satellite machine, there is undesirable growth in the number of leaks.

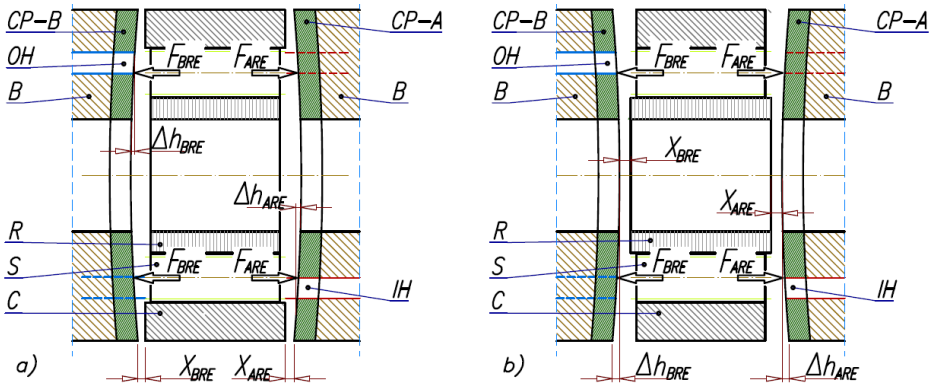

Fig. 9. Deformation of commutation plates CP-A and CP-B as a result of pressure in the working chambers of the satellite machine with a motionless: a) curvature C; b) rotor R: S – satellite, B – body or manifold. Other symbols described in the text

5. Configurations of the compensation unit

To obtain a balance (1) of the commutation plate it is necessary to apply a compensation force F_{CO} to the commutation plate in order to limit unfavourable deformation of the commutation plate and ensure contact of the commutation plate with the fixed (stationary) element of the satellite mechanism (rotor or curvature).

The force F_{CO} is exerted by the action of the compensation pressure p_{CO} on a suitable field A_{CO} on the commutation plate. However, the value of this force cannot exceed a certain level, because excessive force F_{CO} results in the disappearance of the axial clearance of the movable elements of the working mechanism (as discussed below).

In satellite positive-displacement machines, depending on the design solution of this machine, it is possible to balance either one commutation plate or both of them. The shape of compensation field A_{CO} in these machines is important because the correct operation of the compensation unit depends on this shape and its dimensions. Methods of shaping compensation field A_{CO} in satellite machines are presented in Fig. 10 ÷ Fig. 15. Symbols in the following figures are described in Tab. 2. In all figures the compensation fields are in the shape of a ring with two diameters: d_{CO} and D_{CO}.

Tab. 2. Symbols used in Fig. 10 ÷ Fig. 15.

CL	collector
X	cover
G	gasket
KK	compensation channel
HP	inflow (high pressure) channel
LP	outflow (low pressure) channel
D_{CO}, d_{CO}	diameters of compensation field A_{CO}
D''_{CO1}, d''_{CO1}	diameters of compensation field A''_{CO} (Fig. 14)
A''_{CO}	compensation field on the commutation plate CP-B (Fig. 14)

The compensation unit configurations shown in Fig. 10 ÷ Fig. 13 can be applied in satellite machines which can operate in both directions. In contrast, Fig. 14 and Fig. 15 shows the compensation unit configurations for machines that can work in only one fixed direction. That is, only one direction of shaft rotation (Fig. 14) or one direction of body rotation (Fig. 15) is possible. In both cases the port p_H must always be the high pressure port.

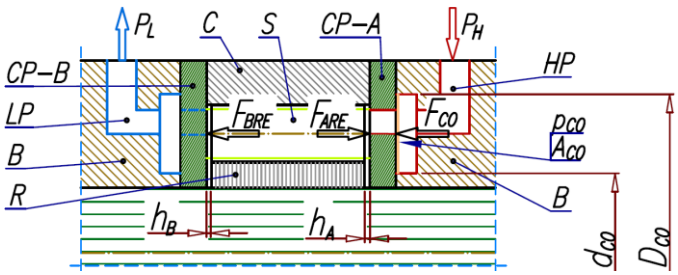

Fig. 10. The compensation of one commutation plate (the plate CP-A – on the inflow channel HP side) in motor with motionless curvature. Height of gaps h_A and h_B as in unloaded motor. Symbols described in Tab. 2

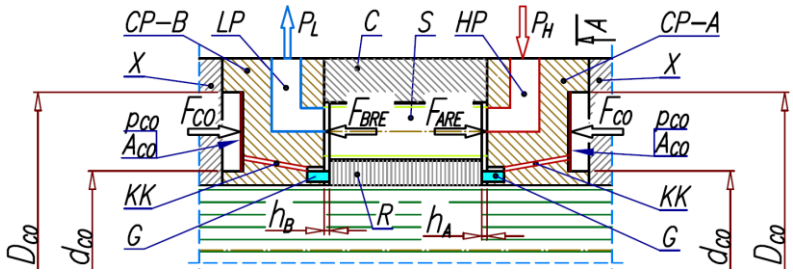

Fig. 11. The compensation of both commutation plates CP-A and CP-B in motor with motionless curvature. The compensation pressure p_{CO} is the same as the pressure under the gasket G (average pressure from high pressure and low pressure working chambers). Height of gaps h_A and h_B as in unloaded motor. Symbols described in Tab. 2

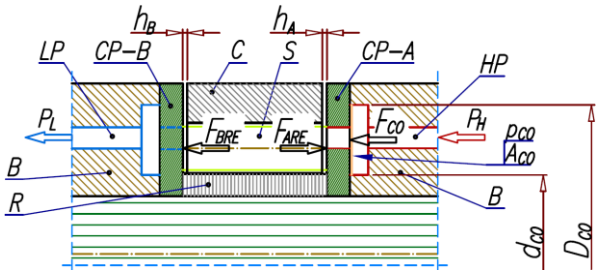

Fig. 12. The compensation of one commutation plate (the plate CP-A – on the inflow channel HP side) in motor with motionless rotor. Symbols described in Tab. 2

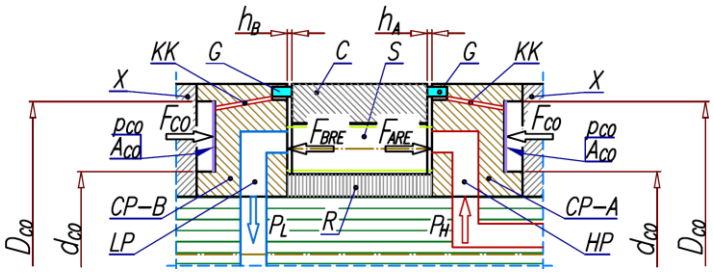

Fig. 13. The compensation of both commutation plates CP-A and CP-B. The compensation pressure p_{CO} is the same as the pressure under the gasket G (average pressure from high pressure and low pressure working chambers). Height of gaps h_A and h_B as in unloaded motor. Symbols described in Tab. 2

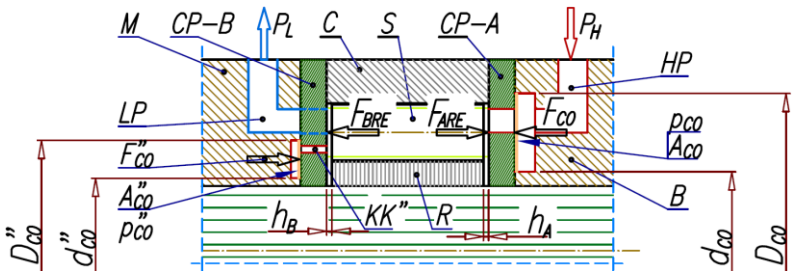

Fig. 14. The compensation of both commutation plates CP-A and CP-B in motor with motionless curvature and one fixed direction of shaft rotation. Height of gaps h_A and h_B as in unloaded motor. Symbols described in Tab. 2

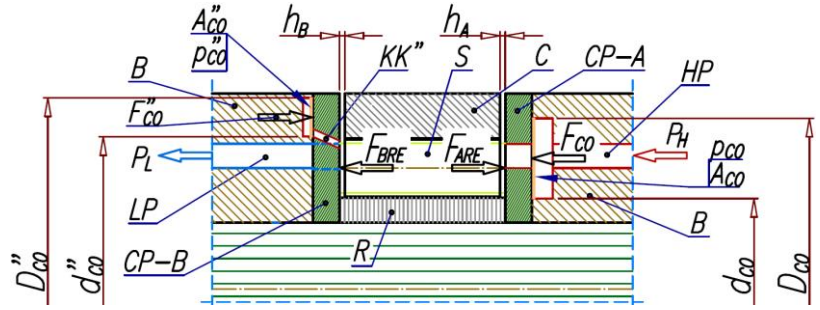

Fig. 15. The compensation of both commutation plates CPA and CP-B in motor with motionless rotor and one fixed direction of body rotation. Height of gaps h_A and h_B as in unloaded motor. Symbols described in Tab. 2

The pressure p_{CO} (Fig. 14 and Fig. 15) in the compensation chamber on the plates CP-A is nearly the same as p_H. The compensation chamber on the plate CP-B is connected with high pressure working chambers HPC by the channel KK". Then, the pressure p''_{CO} is nearly the same as p_{inH}.

6. Determining the geometrical dimensions of compensation field – the equilibrium conditions of the compensation plate and diameters of compensation field

Depending on the value of the compensation field, there may be an increase of axial clearances of the satellites and rotor (or curvature) or a decrease of these axial clearances. In the first case, the finite height of gaps h_{ACO} and h_{BCO} is bigger than h_A and h_B accordingly. It is possible when the compensation field A_{CO} is too small (Fig. 16). As a result of increasing the axial clearances of the working mechanism elements, there will be an increase of leakage and decrease of volumetric efficiency.

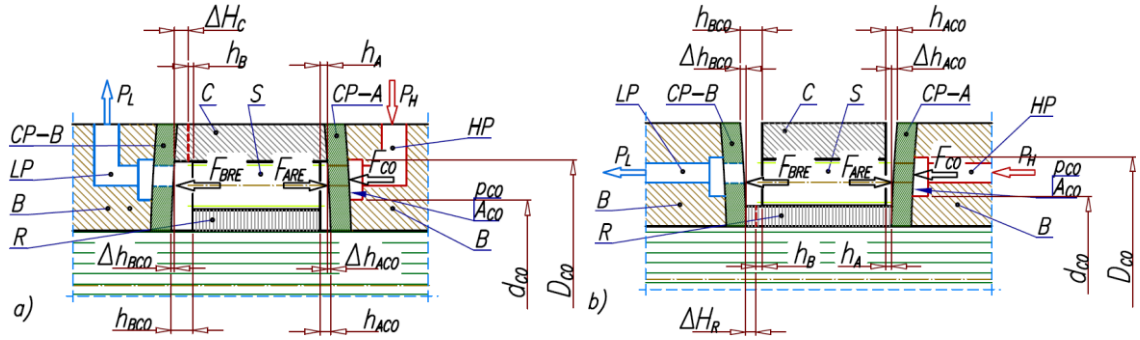

Fig. 16. The increase of height of gaps from h_A and h_B to h_{ACO} and h_{BCO} as a result of too small compensation area A_{CO}: a) in motor with motionless curvature; b) in motor with motionless rotor; ΔH_C and ΔH_R – change in the height of curvature and rotor, Δh_{ACO} and Δh_{BCO} – deflection of compensation plates. Other symbols described in text

However, in the case of reducing axial clearances of working mechanism elements, the following effect occurs:

a) desirable – when in unloaded working mechanism the finite height of gaps h_{ACO} and h_{BCO} is smaller than the height of gaps h_A and h_B (Fig. 17). The result is reduced leakage and increased volumetric efficiency associated with the machine;
b) undesirable – when the finite height of gaps h_{ACO} and h_{BCO} is zero. The results are: loss of leakages, creation of friction between the working mechanism elements and commutation plates, reduction of mechanical efficiency and, eventually, the process of seizing.

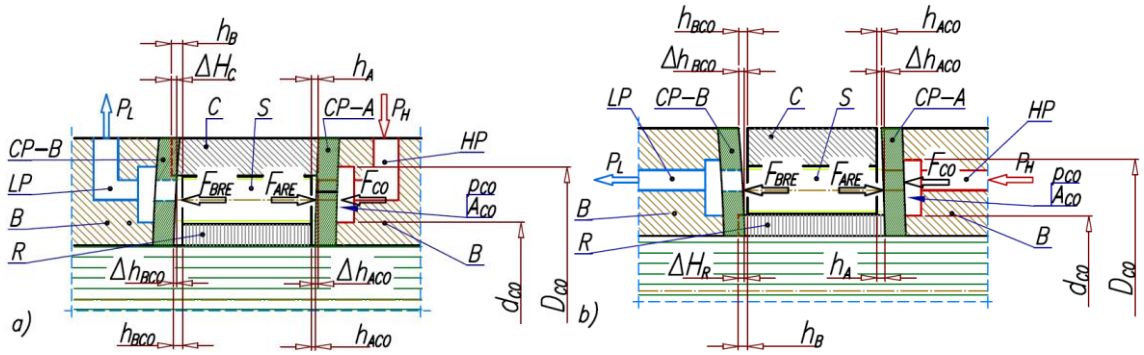

Fig. 17. The reduction of the height of gaps from h_A and h_B to h_{ACO} and h_{BCO} in a motor with correct compensation area A_{CO}: a) in a motor with motionless curvature; b) in a motor with motionless rotor. Symbols like in Fig. 16

The maximum of axial clearance of elements in working mechanism of a satellite motor with axial clearance compensation is:

a) in a motor with a motionless curvature:

$$\Delta h_{C-max} = h_{ACO} + h_{BCO} = h_A + h_B \pm \Delta h_{ACO} \mp \Delta h_{BCO} \pm \Delta H_C \tag{18}$$

b) in a motor with a motionless rotor:

$$\Delta h_{C-max} = h_{ACO} + h_{BCO} = h_A + h_B \pm \Delta h_{ACO} \mp \Delta h_{BCO} \pm \Delta H_R \tag{19}$$

In order to calculate the compensation field and diameters it should be assumed that:

$$M_{CO} \geq M_{RE} \tag{20}$$

where M_{CO} is the moment of compensation force and M_{RE} is the moment of repulsive force.

In order to calculate M_{CO} and M_{RE} the following simplification was adopted:

a) for a mechanism with a motionless curvature – a bending moment of the commutation plate is calculated relatively to the place of support of this plate – that is relative to the so-called reference circle of the curvature with the diameter d_C (Fig. 18c);
b) for a mechanism with a motionless rotor – a bending moment of the commutation plate is calculated relatively to the so-called reference circle of the rotor with the diameter d_R (Fig. 19c).

The name reference circle of the curvature refers to the circle that divides the field of lateral surface of curvature A_C into two equal fields A_{C-1} and A_{C-2} ($A_{C-1} = A_{C-2}$). Similarly, the reference circle of the rotor refers to the circle that divides the field of lateral surface of rotor A_R into two equal fields A_{R-1} and A_{R-2} ($A_{R-1} = A_{R-2}$) (see Fig. 18 and Fig. 19).

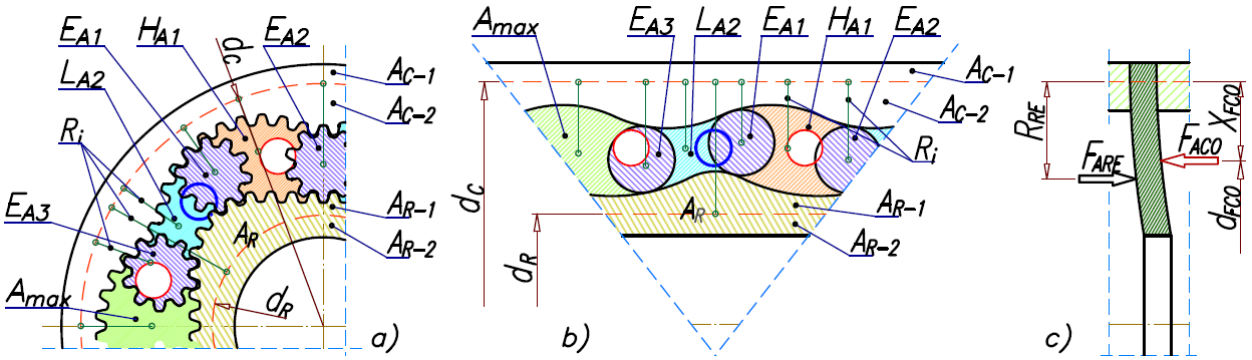

Fig. 18. The method of calculating moments M_{CO} and M_{RE}: a) satellite mechanism with a motionless curvature, b) aligned view of the satellite mechanism, c) forces F_{CO} and F_{RE} that bend the commutation plate. All symbols described in the text

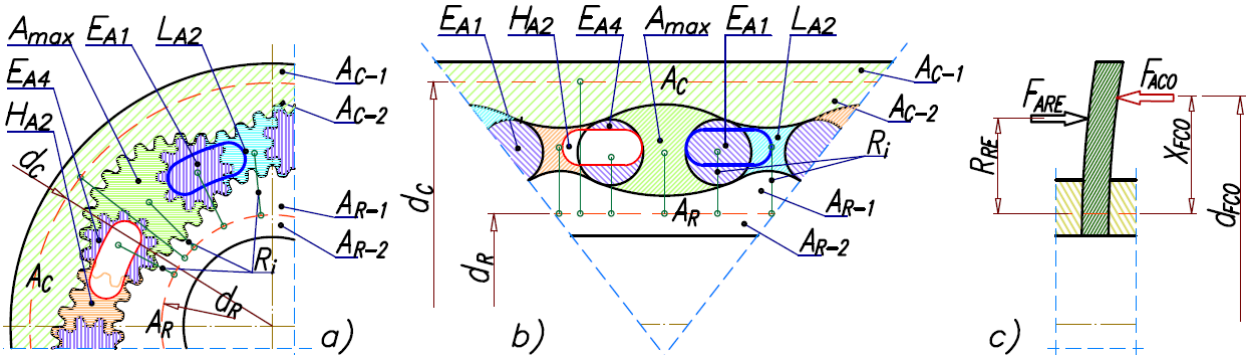

Fig. 19. The method of calculating moments M_{CO} and M_{RE}: a) satellite mechanism with a motionless rotor, b) aligned view of the satellite mechanism, c) forces F_{RE} and F_{CO} that bend the commutation plate. All symbols described in the text

The moment of repulsive force (on the compensated plate CP-A) is:

$$M_{ARE} = \sum R_i \cdot H_{Ai} \cdot p_{inH} + \sum R_i \cdot L_{Ai} \cdot p_{inL} + \sum R_i \cdot E_{Ai} \cdot p_{av} + \frac{d_C - d_R}{2} \cdot A_R(A_C) \cdot p_{av} \tag{21}$$

This formula is true both for a mechanism with motionless curvature (A_R is taken into account) and for a mechanism with motionless rotor (A_C is taken into account). In this formula, the R_i is the radial distance between the center of the pressure field and the reference circle. If the plate CP-B is compensated the procedure of calculation M_{BRE} will be similar.

The moment of compensation force is:

$$M_{ACO} = X_{FCO} \cdot F_{ACO} = X_{FCO} \cdot A_{CO} \cdot p_{CO} \tag{22}$$

From the criterion (1) it follows that:

$$A_{CO} \geq \frac{F_{ARE}}{p_{CO}} = A_{RE} \tag{23}$$

where A_{RE} is the value of the field reduced to the compensation pressure p_{CO}.

The diameter d_{CO} (Fig. 18 and Fig. 19) is defined as the diameter of the reference circle of the compensation field. This circle (similarly as in the reference circle of the curvature and rotor) divides the compensation field A_{CO} (Fig. 10) into two equal fields that is:

$$\frac{\pi}{4} \cdot \left({d_{FCO}}^2 - {d_{CO}}^2 \right) = \frac{\pi}{4} \cdot \left({D_{CO}}^2 - {d_{FCO}}^2 \right) = \frac{1}{2} \cdot A_{CO} \tag{24}$$

from which:

$$A_{CO} = \frac{\pi}{2} \cdot \left({D_{CO}}^2 - {d_{CO}}^2 \right) = \frac{\pi}{2} \cdot \left({d_{FCO}}^2 - {d_{CO}}^2 \right) \tag{25}$$

Furthermore:

a) for a mechanism with motionless curvature:

$$d_{FCO} = d_C - 2 \cdot X_{FCO} \tag{26}$$

b) for a mechanism with motionless rotor:

$$d_{FCO} = d_R + 2 \cdot X_{FCO} \tag{27}$$

From the Fig. 18c and Fig. 19c it follows that:

$$R_{RE} \cdot F_{ARE} = M_{ARE} \tag{28}$$

From the above formula and from formulas (20) and (22) it follows that:

$$X_{FCO} = R_{RE} = \frac{M_{ARE}}{F_{ARE}} \tag{29}$$

Whereas from the formulas (24) ÷ (29) it follows that:

a) for a mechanism with motionless curvature:

$$d_{CO} \leq \sqrt{\left(d_C - 2 \cdot \frac{M_{ARE}}{F_{ARE}}\right)^2 - \frac{2}{\pi} \cdot A_{RE}} \tag{30}$$

$$D_{CO} \geq \sqrt{\left(d_C - 2 \cdot \frac{M_{ARE}}{F_{ARE}}\right)^2 + \frac{2}{\pi} \cdot A_{RE}} \tag{31}$$

b) for a mechanism with motionless rotor:

$$d_{CO} \leq \sqrt{\left(d_R + 2 \cdot \frac{M_{ARE}}{F_{ARE}}\right)^2 - \frac{2}{\pi} \cdot A_{RE}} \tag{32}$$

$$D_{CO} \geq \sqrt{\left(d_R + 2 \cdot \frac{M_{ARE}}{F_{ARE}}\right)^2 + \frac{2}{\pi} \cdot A_{RE}} \tag{33}$$

It should be taken into account that during the design of a compensation unit in a satellite machine, design or technological factors limiting the diameter D_{CO} or the diameter d_{CO} will occur. In this regard, one of these diameters will be determined from top-down. Therefore, two cases should be considered: the diameter d_{CO} or D_{CO} is known.

In the first case it is necessary to find the diameter D_{CO}. Then, from equation (24):

$$D_{CO} = \sqrt{2 \cdot {d_{FCO}}^2 - {d_{CO}}^2} \tag{34}$$

After substituting (25) into (22) and then (22) into (20), the following formula is obtained:

$$M_{ARE} = \frac{\pi}{2} \cdot X_{FCO} \cdot \left({d_{FCO}}^2 - {d_{CO}}^2\right) \cdot p_{CO} \tag{35}$$

Subsequently, after substituting X_{FCO} from (26) and (27), respectively, into (35) and transformation, the following results are obtained:

a) for a mechanism with motionless curvature:

$$\frac{4}{\pi} \cdot \frac{M_{ARE}}{p_{CO}} = (d_C - d_{DCO}) \cdot \left({d_{FCO}}^2 - {d_{CO}}^2\right) \tag{36}$$

b) for a mechanism with motionless rotor:

$$\frac{4}{\pi} \cdot \frac{M_{ARE}}{p_{CO}} = (d_{FCO} - d_R) \cdot \left({d_{FCO}}^2 - {d_{CO}}^2\right) \tag{37}$$

The diameter of d_{FCO} should be calculated from the formulas (36) and (37). Due to the fact that they are third-degree equations, they should be solved by numerical methods or by the method of subsequent approximations. If the diameter d_{FCO} is calculated, the diameter D_{CO} should be calculated from formula (34).

In the second case, it is necessary to find the diameter d_{CO}. Then, from equation (24):

$$d_{CO} = \sqrt{2 \cdot {d_{FCO}}^2 - {D_{CO}}^2} \tag{38}$$

After substituting (38) into (28) and (22) and then into (20), the following formula is obtained:

$$M_{ARE} = \frac{\pi}{2} \cdot X_{FCO} \cdot \left({d_{FCO}}^2 - {D_{CO}}^2\right) \cdot p_{CO} \tag{39}$$

Next, after substituting X_{FCO} from the equations (26) and (27), respectively, into (39) and transformation, the following result is obtained:

a) for a mechanism with motionless curvature:

$$\frac{4}{\pi} \cdot \frac{M_{ARE}}{p_{CO}} = (d_C - d_{FCO}) \cdot \left({d_{FCO}}^2 - {D_{CO}}^2\right) \tag{40}$$

b) for a mechanism with motionless planet:

$$\frac{4}{\pi} \cdot \frac{M_{ARE}}{p_{CO}} = (d_{FCO} - d_R) \cdot \left({d_{FCO}}^2 - {D_{CO}}^2\right) \tag{41}$$

The diameter of d_{FCO} should be calculated from the formulas (40) and (41) by numerical methods or by the method of subsequent approximations. If the diameter d_{FCO} is calculated, the diameter d_{CO} should be calculated from the formula (38).

Diameters chosen this way may differ from the ones obtained numerically. Furthermore, for such selected diameters of compensation field the condition of the tightness in area where compensation plate contacts the motionless elements of working mechanism (with the curvature or with the rotor) is not ensured. Therefore, the downforce in the area of contact should be increased by:

a) increasing the D_{CO} diameter for a mechanism with motionless curvature ;
b) decreasing the d_{CO} diameter for a mechanism with a motionless rotor.

Thus, taking into account the correction from numerical calculations, it is proposed to write formula (34) as:

$$D_{CO} = C_{DCO} \cdot \sqrt{2 \cdot {d_{FCO}}^2 - {d_{CO}}^2} \tag{42}$$

whereas formula (38) in the form:

$$d_{CO} = \frac{1}{C_{dCO}} \cdot \sqrt{2 \cdot {d_{FCO}}^2 - {D_{CO}}^2} \tag{43}$$

where C_{DCO} and C_{dCO} are correction coefficients. Based on previous experience, it is proposed to adopt $C_{DCO}=C_{dCO}=1.15$.

Compensation diameters D_{CO} and d_{CO} calculated according to formulas (30)÷(33) or (42) and (43) are preliminarily accepted diameters in the process of satellite machine design. These diameters and the same values of coefficients C_{DCO} and C_{dCO} can be verified by numerical calculation (calculation of the deformation of machine elements). The numerical calculation results should be verified experimentally.

7. Experimental methods of verifying the compensation unit operation

Experimental methods allow for testing the correctness of the commutation unit operation. These experimental methods are:

a) a measurement of the change in distance between commutation plates in the whole range of possible load for the satellite machines;
b) a measurement of leakage Q_{Lfg-1} (as an external leakage):
   – for a machine with motionless curvature – only in gaps between the rotor and compensation plates;

– for a machine with a motionless rotor – only in gaps between the curvature and compensation plates;

c) a measurement of torque – when the axial clearances disappear, the friction in working mechanism occurs and the value of torque decreases.

Accordingly, it is possible to determine the leakage in flat gaps between satellites and compensation plates (as an internal leakage):

$$Q_{Lfg-2} = Q_{out} - q_t \cdot n \tag{44}$$

where:

– Q_{out} – flow rate measured in the outflow pipe (see Fig. 29),
– q_t – theoretical displacement of motor,
– n – rotational speed of motor.

The sum of Q_{Lfg-1} and Q_{Lfg-2} yields the total leakages Q_{Lfg} (Fig. 20) in flat gaps of the satellite working mechanism:

$$Q_{Lfg} = Q_{Lfg-1} + Q_{Lfg-2} \tag{45}$$

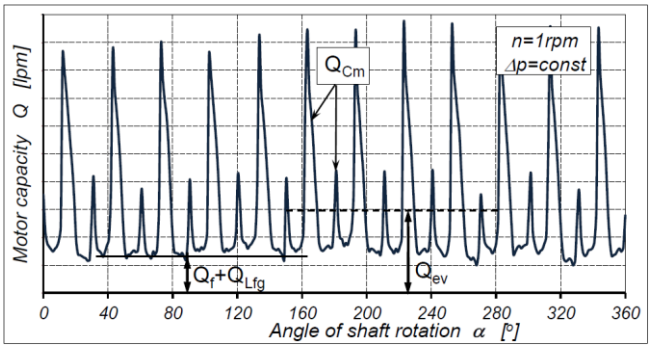

Fig. 20. Characteristics Q = f(α) of total flow rate in loaded satellite motor at low constant speed [26,32]: Q_{Cm} – flow rate in commutation unit clearances, Q_{ev} – average flow rate. Other symbols described in the text

Theoretical characteristics of leakages Q_{Lfg} are shown in Fig. 21, where Δp_{in} is the difference of pressure in the working chambers. Due to the low rotational speed of the machine, the flow rate in this machine is small. Thus, the pressure drop in internal channels can be omitted. Therefore, it can be assumed that [26,27,28,29]:

$$\Delta p_{in} = \Delta p = p_H - p_L \tag{46}$$

where Δp is the difference of pressure measured in the inflow and outflow ports of the machine.

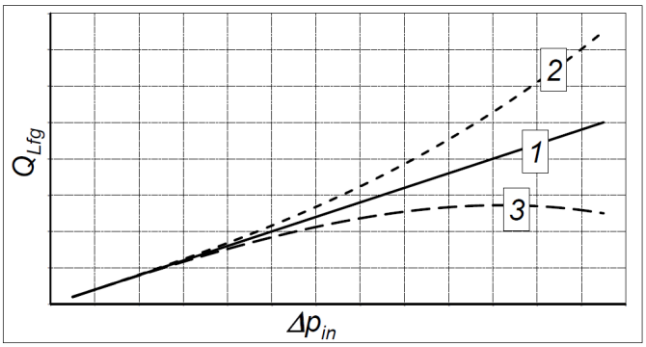

Fig. 21. Characteristics of leakages Q_{Lfg} in flat gaps of the satellite working mechanism. The description in text [17,32]

The measurement of leakages in flat gaps in a satellite machine is carried out during the tests of the machine with low constant rotational speed (for example with n = 1 rpm) [26,27,28,29]. During this test, the pressure in the machine is increased and leakages are measured and the torque

is observed. If the value of leakages decreases significantly and the value of torque is too low, there is high friction of the working mechanism elements against the commutation plate.

Characteristics presented in Fig. 21 should be interpreted as follows:

a) the characteristic No. 1 can occur in two cases, that is:
   - a constant height of gaps in the working mechanism and laminar liquid flow in gaps, e.g. mineral oil flow;
   - a slight increase in the height of gaps in the mechanism and not fully developed turbulent liquid flow in gaps. This case with this kind of flow has been observed during testing the hydraulic motor with pure tap water (water has very low viscosity, over forty times smaller than the viscosity of mineral oil) [27,32];
b) the characteristic No. 2 – an increase in the height of gaps and any type of liquid flow in gaps;
c) the characteristic No. 3 – refers to two cases, that is:
   - reducing the height of the gaps for any type of liquid flow in these gaps;
   - maintaining a constant height of the gaps and changing the type of liquid flow – from laminar flow to not fully developed turbulent flow [27,32].

Thus, the characteristics No. 1 and No. 3 result from the operation of a clearance compensation unit in a satellite machine. The characteristic No. 2 is significant for satellite machines without a compensation unit.

In practice, it is sufficient to measure the leakage $Q_{Lfg\text{-}1}$, because the height of gaps between the curvature and compensation plates (for motor with a motionless rotor) or between the rotor and compensation plates (for motor with a motionless curvature) is the biggest change.

8. The axial clearance compensation unit in a satellite motor with a motionless rotor

8.1. Satellite motor

The new design of a satellite motor with rotating body is shown in Fig. 22. This motor is equipped with a satellite mechanism as in Fig. 2 (the teeth module is m = 1.5 mm and geometrical displacement is 48 cm^3/rev) and equipped with an axial clearance compensation unit according to the schematic drawing shown in Fig. 12 and Fig. 17b. In this motor, the body 1 (Fig. 22) drives any device, e.g. winch drum, driving wheel of vehicle etc. Thus, the curvature C rotates in this motor. For this reason, both commutation plates (CP-A and CP-B) are equipped with four inflow/outflow holes as in Fig. 6, Fig. 7 and Fig. 19. This motor can be powered by port A or port B depending on the desired direction of rotation. Therefore, only one commutation plate can be compensated – only the plate on the side of the high pressure internal channel (port A or port B – Fig. 22). In this motor, leakage from the curvature gaps is discharged by third channel (Fig. 22). The compensation plates CP-A and CP-B, rotor R and rear manifold 5 are clutched by the nut 6. Therefore, regardless of the value of the motor load, the condition (1) is met and there is no situation as in Fig. 9b) and there is no leakage into the space around pin 2.

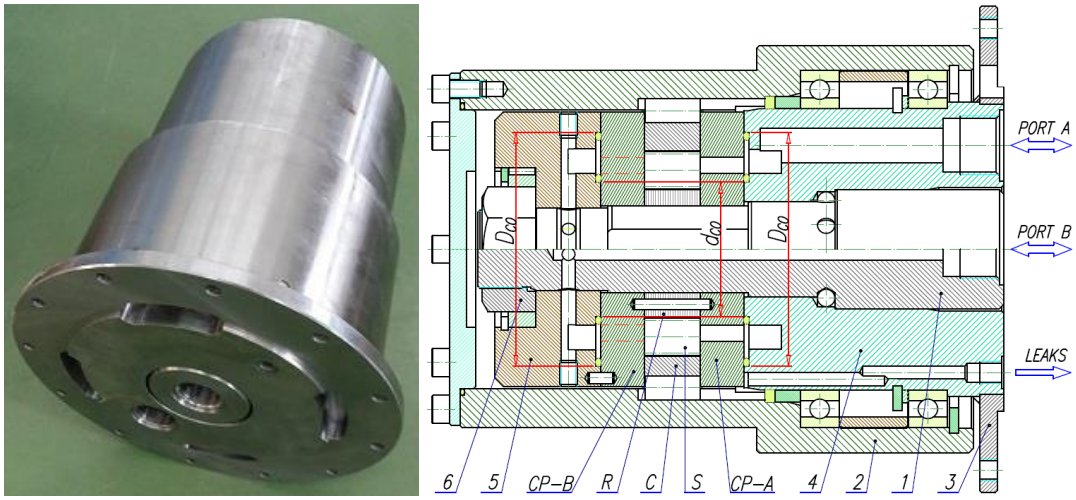

Fig. 22. The satellite motor with rotating body [30,31,32]: C – curvature, R – rotor, S – satellites, CP-A and CP-B – commutation plates, 1 – body, 2 – pin, 3 – mechanical connector of motor, 4 – front manifold, 5 – rear manifold, 6 – nut, D_{CO} and d_{CO} – diameters of compensation field

In presented motor, it is possible to increase the geometrical displacement only by increasing the height of the working mechanism (that is the height of the curvature C, the rotor R, and satellites S) and employing an appropriate extension of the pin 1. This operation will cause a significant increase in the torque with a slight increase in the motor mass. Therefore, the motor, due to its small size and weight, will be able to be built into lighter and simplified devices. The big advantage of the motor is that the body can be loaded with radial forces and can be an element of a driven machine. For example, the motor without a body can be installed directly in a hoisting winch.

The diameters D_{CO} and d_{CO} of compensation field should be calculated for such an angular position of the working mechanism that the maximum repulsive force is obtained. This is the position that is shown in Fig. 5c and Fig. 6c. The values of the pressure fields on the compensation plate are given in Tab. 3.

Tab. 3. Values of pressure fields in [mm^2] on the compensation plate CP-A according to Fig. 6c and Fig. 7c.

A_o	L_{A1}	L_{A2}	H_{A1}	H_{A2}	E_{A1}	E_{A2}	E_{A3}
3806.52	283.76	137.92	500.60	138.08	179.64	156.88	144.12

Characteristics of repulsive force in satellite mechanism, calculated according to formula (14) and assuming that p_{inH} = 25 MPa and p_{inL} =0.2 MPa, are shown in Fig. 23.

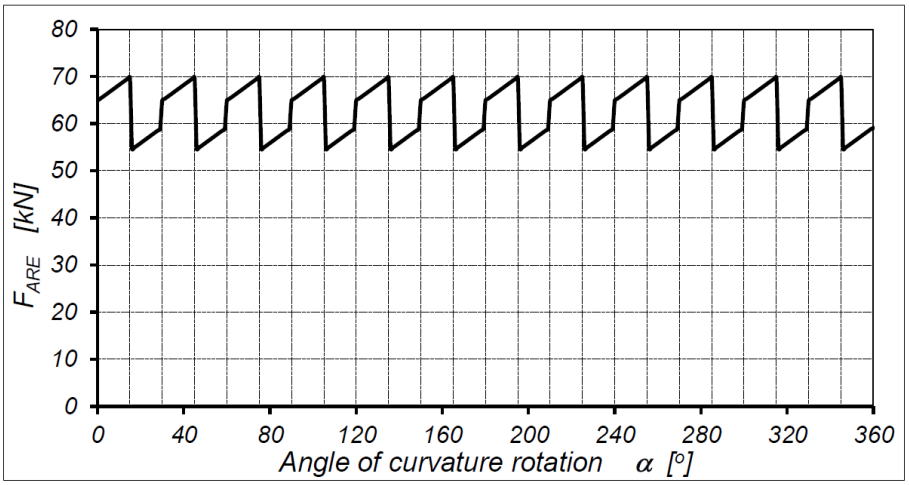

Fig. 23. Characteristics of repulsive force $F_{ARE}=f(\alpha)$ calculated according to formula (14) at p_{inH} = 25 MPa and p_{inL} = 0.2 MPa

The diameters of the compensation field, calculated according to formulas (32) and (33), are: $d_{CO} \leq 77.9$ mm and $D_{CO} \geq 111.3$ mm. However, during the design process of the motor, it was found that the above theoretical diameters are not correct due to the location of the inflow and outflow holes in the commutation plates. This way, the diameter d_{CO} was decreased (d_{CO} = 62.0 mm). Then, the diameter D_{CO} was recalculated according to the formulas (34) and (37) (D_{CO} = 106.4 mm).

Furthermore, it was assumed that the post-assembly axial clearances of the rotor and satellites equal 20 μm, that is h_A+h_B = 20 μm.

8.2. Numerical calculations of the compensation unit

The FEM analysis allows to find changes of axial clearances due to the load of the working mechanism, that is an increase of the axial clearances between the satellites and the curvature, or decreases of the axial clearances and a clamp of the satellite and rotor by the commutation plate.

Elements of the motor which are deformed as a result of pressure, are divided into finite elements (Fig. 24). That is:

a) the pin (Fig. 24) and manifolds are divided into four-sided elements with an edge of 5 mm – this dimension allowed to achieve satisfactory results with relatively low computational complexity;
b) the rotor (Fig. 24) is divided into six-sided elements with the edge of 3 mm – it ensures a good transfer of load in contacts between the rotor and compensation plates;
c) the nut is divided into six-sided elements with the edge of 5 mm – such a large dimension of finite element is sufficient because information about deformation of the nut is not needed;
d) compensation plates (Fig. 24) are divided into four-sided elements with the edge of 2 mm – such a small length of edges allowed to precisely determine the size of their deformations.

The curvature and satellites are embedded in the motor with a clearance. Therefore, they are omitted in the solid model. However, on the commutation plate there is the average pressure field whose shape corresponds to the shapes of curvature and satellites (Fig. 25).

Fig. 24. The commutation plate, pin and rotor divided into finite elements [31]

Pressure is the main factor exerting loads on the elements in a motor. For numerical calculation it was assumed that the satellite motor is supplied by port A. In such case, the pressure distribution on the commutation plate CP-A is as shown in Fig. 25. The angle position of the curvature is taken to obtain the largest high pressure fields (Fig. 25a). Next, the maximum repulsive force F_{ARE} is obtained.

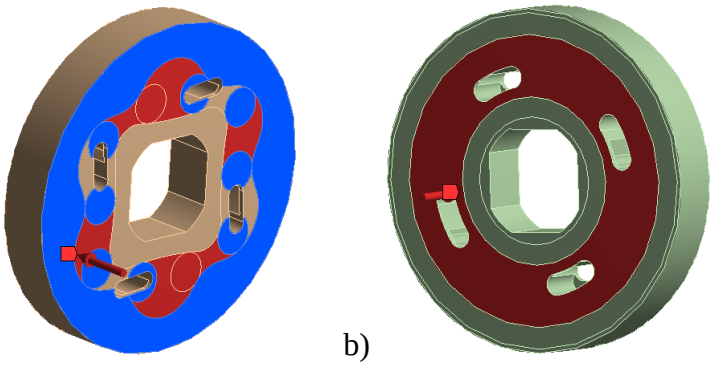

a) b)

Fig. 25. The pressure distribution on the commutation plate CP-A [31]: a) on the side of the working mechanism – the pressure is 25 MPa (red colour) and 12.5 MPa (blue colour), b) on the side of front manifold – the pressure is 25 MPa. Red arrows – the direction of pressure set in the ANSYS program

The motor was supported along the edge of the front manifold (Fig. 26). This support takes away six degrees of freedom. In addition, a layer of contact elements was introduced between all the contacting elements. A contact type „Bonded" simulating a threaded connection was introduced between the pin and the nut. The same type of contact was introduced between the back manifold and the nut because these elements will always remain in permanent contact and it would be useless to introduce the non-linear constant (longer calculation time). All contacts between the pin and other elements are type „Frictionless". Contact type „Frictional" occurs:

a) between the front manifold and the compensation plate CP-A;
b) between the rear manifold and the compensation plate CP-B;
c) between the rotor and compensation plate CP-A and between the rotor and compensation plate CP-B.

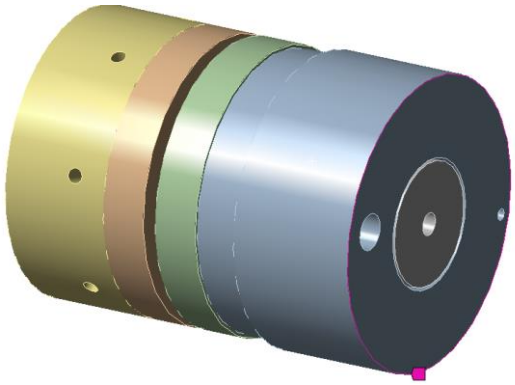

Fig. 26. The support (purple circle) of motor model on the edge of front manifold [31]

Only three series of calculations were carried out – for different diameters D_{CO} and for one constant supply pressure 25 MPa [31]. The final results of FEM calculations showed that:

a) the deformation of commutation plates are in accordance with the sketch given in Fig. 17b);
b) the deformation of commutation plates is not symmetrical and does not exceed 27 μm (Fig. 27 and Fig. 28). [31]. It is a result of the distribution of high and low pressure fields on the commutation plates (Fig. 25a);
c) the maximum decreasing of distance between the commutation plates is 10 μm (Fig. 27 and Fig. 28). That is the minimum value of axial clearance of curvature is not less than 10 μm;
d) the following compensation diameters: d_{CO} = 62.0 mm and D_{CO} = 112.0 mm should be applied in the motor;
e) the post-assembly height of gaps in the working mechanism (the axial clearance of the satellite and curvature with the value of 20 μm) that was assumed in the project is correct.

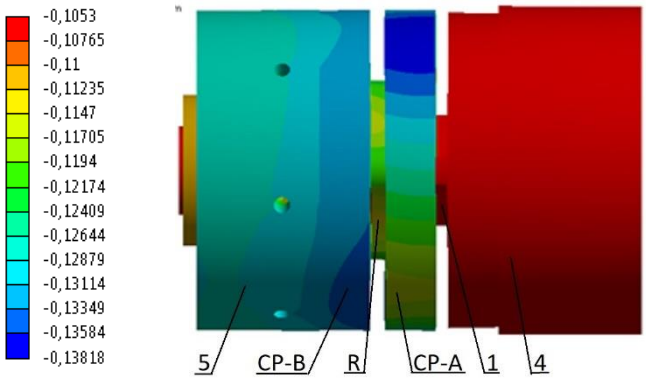

Fig. 27. Deformations of motor parts in [mm] in the axial direction [31]: R - rotor, CP-A and CP-B – compensation plates, 1 – pin, 4 – front manifold, 5 – rear manifold

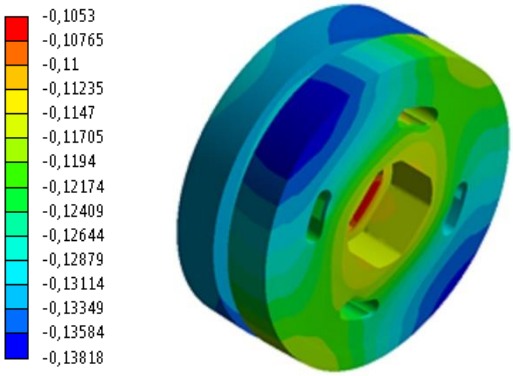

Fig. 28. Deformations of the commutation plates in [mm] in the axial direction [31]

The gap between the compensation plate CP-A and front manifold 4 (Fig. 27) is a results from the elastic extension of the pin 1 under pressure. This gap is not dangerous for the motor because special gaskets are fitted between the compensation plate CP-A and front manifold 4.

8.3. Experimental verification of the correctness of operation of the axial clearance compensation unit

The correctness of the axial clearance compensation unit operation can be verified by the measurement of the leaks Q_{Lfg-1} in the curvature gaps (gaps between the curvature and the commutation plate) and by the measurement of torque M. Leaks Q_{Lfg-1} from the tested motor are discharged through the third channel (Fig. 22 – channel "Leaks"). Such tests are recommended to be carried out at a low, constant rotational speed of the hydraulic motor (no more than several revolutions per minute) [26,27,29,31]. This way, the body of motor was coupled with worm gear WG with the ratio of 1:120 at the test stand (Fig. 29). This gear was driven by an electric motor E. The measurement of leaks Q_{Lfg-1} (flowmeter Q_{Lfg-1} in Fig. 29) and the measurement of torque M should be performed with constant pressure drop Δp in the motor. The torque M is measured by force transducer FT (range 0÷500 N, class 0.1) mounted on the arm with a length of 0.5 m (the second end of the arm is attached to the pin of the motor). A constant pressure drop Δp in the motor is maintained by the variable displacement pump P and accumulator A (Fig. 29). Mass flow meters with range of 2 lpm and class 0.1 were used for the measurement of flow Q_{Lfg-1} and Q_{out}.

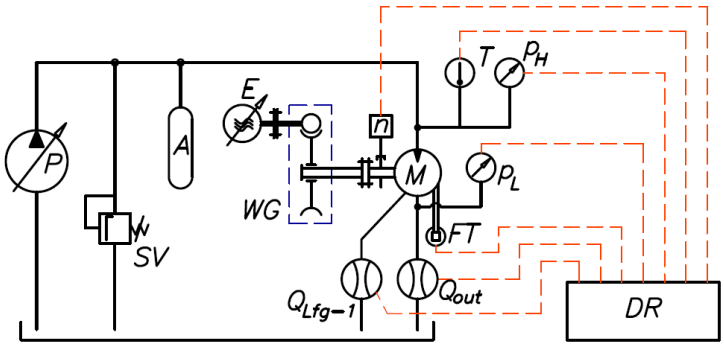

Fig. 29. Schematic drawing of the measurement system on the test stand: M – tested motor, P – pump, A – accumulator, E – electric motor with frequency converter, SV – safety valve, WG – worm gear, DR – data recorder, Q_{out} and Q_{Lfg-1} – flowmeters, FT – force transducer, p_H and p_L – pressure transducers, T – temperature sensor, n – speed transducer

The motor tests were carried out with the following parameters [31]:

- rotational speed – 1 rpm (measured by the inductive sensor, accuracy of measurement ±0,01rpm);
- the pressure p_H in the inflow port A – up to 25 MPa (measured by the strain gauge pressure transducers, range 0÷25 MPa, class 0.3);
- the pressure p_L in the outflow port B – up to 0.6 MPa (measured by a strain gauge pressure transducer, range 0÷1 MPa, class 0.3);
- the viscosity of mineral oil – 40 cSt (corresponding to the oil temperature 43 °C).

The results of the research have shown that:

a) when the pressure drop Δp in the motor increases, the leakages Q_{Lfg-1} in gaps between the curvature and commutation plates are limited (Fig. 30);
b) the value of measured torque M is smaller than theoretical torque by maximum 20% (Fig. 31). It is typical for satellite motor working at low speed [17];
c) there is a lack of regular friction traces of the curvature against commutation plates. This was found after the motor was disassembled (Fig. 32).

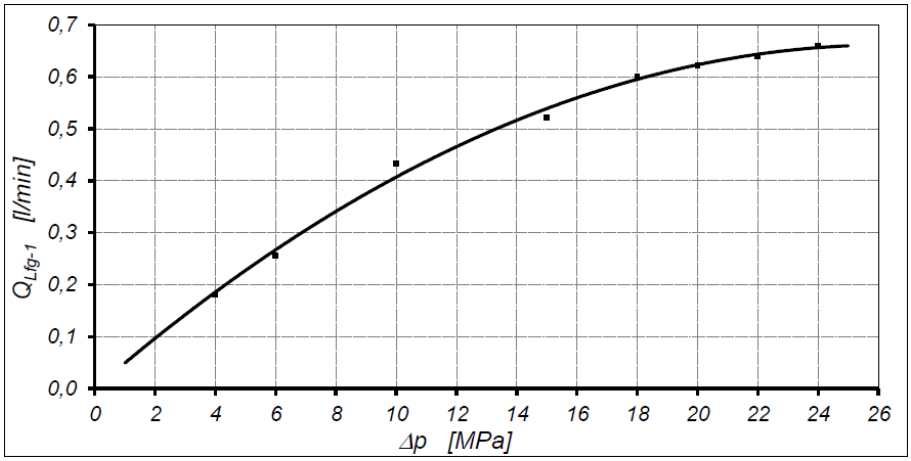

Fig. 30. Characteristics of leakages $Q_{Lfg-1} = f(\Delta p)$ in gaps between the curvature and commutation plates (the leakage is discharged by the third hose) at n = 1 rpm [31]

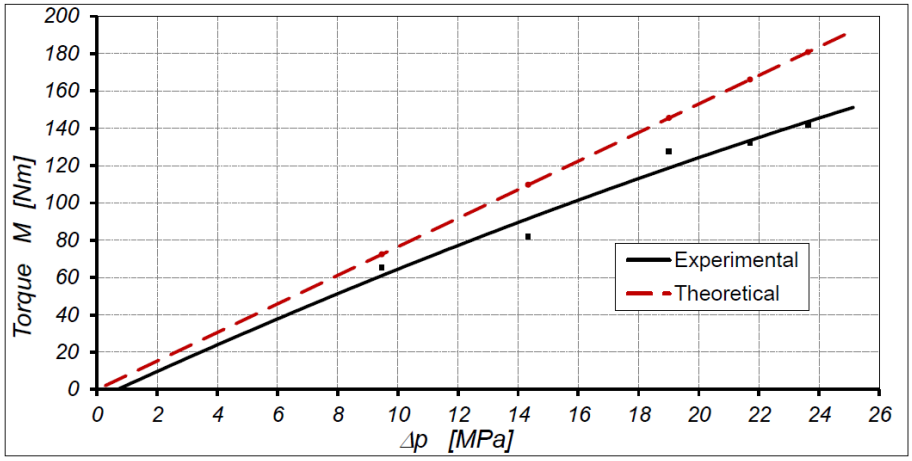

Fig. 31. Characteristics of the average value of torque $M = f(\Delta p)$ of the motor at n = 1 rpm [31]

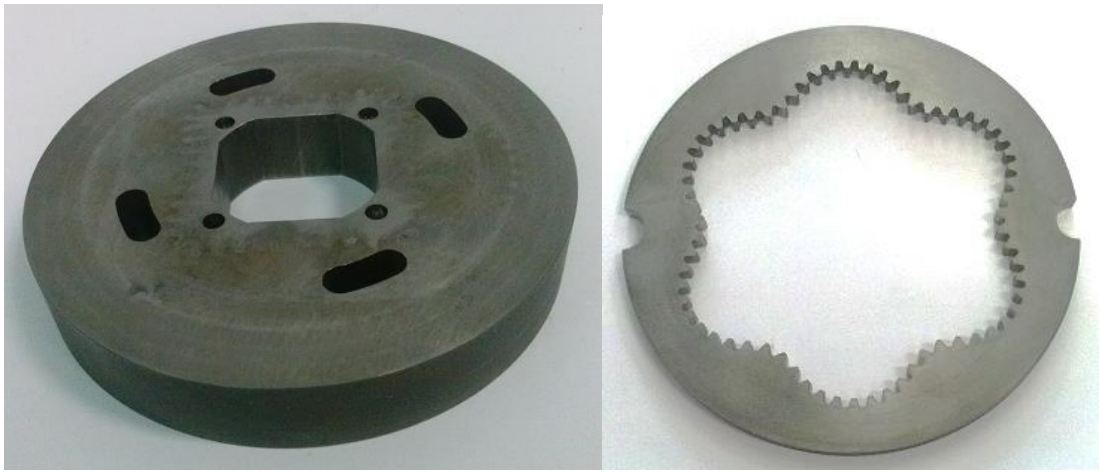

Fig. 32. The compensation plate and the curvature after tests of the motor [31]

9. Conclusions

The main aim of the method of designing an axial clearance compensation unit in any positive displacement satellite machines is the calculation of the diameters of compensation field on a compensation plate and, thus, balancing the moments bending this plate. The first bending moment is a moment of force repulsing a compensation plate, while the second is a moment of compensation force. The repulsive force is a force obtained from pressure in satellite mechanism and acting on the compensation plate. However, the compensation force is generated by compensation pressure acting on a compensation area on the compensation plate on the other side of this plate. The repulsive force and compensation force have the same direction but opposite turn. It is recommended to find the maximum value of the repulsive force. This maximum exists for one specific angle position of curvature in relation to the rotor – at the same time the high pressure fields on the compensation plate are also maximum. It is important, because for the other angular configuration of satellite mechanism, a smaller value of the repulsive force can be obtained. For this situation the calculated compensation field on the compensation plate will be too small. This way, for other angular position of working mechanism than corresponding to the maximum value of high pressure fields, the axial clearances in working mechanism will increase as a result. Therefore, it is preferable to calculate the compensation diameters for the maximum repulsive force. In this case, when the working mechanism has random angular position, the compensation plate can be bending in the direction of decreasing axial clearances which is advantageous because internal leakage is reduced.

It should be taken into account that during the design of a compensation unit in a satellite machine, design or technological factors that limit one of the compensation diameters will occur.

In this regard, one of these diameters will be determined from top-down – the outside diameter or the inside diameter. In addition, it is worth noting that in a motor driven in both directions it is sufficient to calculate the compensation diameters only for one compensation plate. For the second plate, the compensation field must have the same dimensions.

The analytical method allows to calculate the compensation diameters in an approximate way. Therefore, these diameters are calculated with an error. This error occurs mainly due to the simplification involving the average pressure on all lateral surfaces of the curvature and satellites or on all lateral surfaces of rotor and satellites (depending on the type of working machine: with a motionless curvature or with a motionless rotor). The numerical calculation results can be indicated as a proof – on the lateral surface of the curvature there is no constant pressure. In the motor described in this paper, the compensation diameters calculated according to the presented method are 62 mm and 106,4 mm. However, the numerical calculation results showed that for the constant inside diameter (62 mm) the outside diameter will be 112 mm. Thus, the analytical method gives a result that is approximately 5% different from the FEM method. It is a good result. With this approach to this problem, the number of numerical calculation cycles has been limited to only three. This way, the analytical method is advantageous because there is a limited number of numerical calculations and the cost of a project is reduced as a result.

The correctness of the described methods (analytical and FEM) of designing an axial clearance compensation unit was confirmed by experimental tests of the prototype of a satellite motor with rotating body. The axial clearance compensation unit in the tested motor operates correctly.

According to the method described in this paper, it is possible to design an axial clearance compensation unit in any type of positive displacement satellite machines, i.e. in a pump or in a motor and with a motionless curvature or a motionless rotor.

References

1. C. Dymarski, P. Dymarski, Developing Methodology for Model Tests of Floating Platforms in Low-Depth Towing Tank, Archives of Civil and Mechanical Engineering 1 (2016), https://doi.org/10.1016/j.acme.2015.07.003.
2. A. Guzowski, A. Sobczyk, Reconstruction of hydrostatic drive and control system dedicated for small mobile platform, in: Proc. American Society of Mechanical Engineers, Control of Fluid Power Systems Conf., 2014, doi: 10.1115/FPNI2014-7862.
3. P. Walczak, A. Sobczyk, Simulation of water hydraulic control system of francis turbine, in: Proc. American Society of Mechanical Engineers. Coupled Simulation in Mechanical Machines Conf., FPNI2014-78142014, https://doi.org/10.1115/FPNI2014-7814.
4. J. Pobedza, A. Sobczyk, Properties of high pressure water hydraulic components with modern coatings. Materials Engineering and Technology, Advanced Materials Research, Trans Tech Publications Ltd. 849 (2014), https://doi.org/10.4028/www.scientific.net/AMR.849.100.
5. J. Pobedza, A. Sobczyk, Modern coating used in high pressure water hydraulic components. Advanced Materials in Machine Design, Key Engineering Materials 542 (2013), https://doi.org/10.4028/www.scientific.net/KEM.542.143.
6. M. Stosiak, W. Kollek, P. Osiński, P. Cichon, A. Wilczynski, Problems relating to high-pressure gear micropumps, Archives of Civil and Mechanical Engineering 1 (14) (2014), https://doi.org/10.1016/j.acme.2013.03.005.
7. P. Osinski, G. Chruscielski, Strength calculations of an element compensating circumferential backlash in the external gear pump, Journal of Theoretical and Applied Mechanics 1 (54) (2016), doi: 10.15632/jtam-pl.54.1.251.
8. K. Elgert, Ph.D. thesis: Research of axial clearance compensation in hydraulic satellite motors, Gdansk University of Technology, 2010.
9. W. Kollek, Modelling and design of gear pumps. Wroclaw University Publishing House, 2009r.

10. W. Kollek, Gear pumps, construction and exploitation, Ossolineum, Wroclaw, 1996.
11. K. Elgert, A. Balawender, The way of reducing the volumetric losses in hydraulic motors, in: Proc. 2nd International Scientific Forum Developments in Fluid Power Control of Machinery and Manipulators. Fluid Power Net. Int. Cracow University of Technology, 2000.
12. K. Elgert, Satellite hydraulic motor with axial clearance compensation, in: Proc. 2nd International PhD Symposium on Fluid Power, Modena, Italy, 2002.
13. G. Pahl, W. Beitz, J. Feldhusen, K. Grote, Engineering Design. A Systematic Approach. 3rd edition, Springer-Verlag London, 2007. DOI: 10.1007/978-1-84628-319-2.
14. D. F. Moore, Viscoelastic Machine Elements, Chapter: Design methodology. Elsevier, 1993. DOI: 10.1016/C2009-0-24354-6.
15. P. Stryczek, M. Banaś, F. Przystupa, Design And Research On A Hydraulic Cylinder With Plastic Components. Conference: 9th FPNI Ph.D. Symposium on Fluid Power, Florianópolis, SC, Brazil, October 26–28, 2016. Paper No. FPNI2016-1508. DOI: 10.1115/FPNI2016-1508.
16. J. Stryczek, S. Bednarczyk, K. Biernacki, Strength analysis of the polyoxymethylene cycloidal gears of the gerotor pump. Archives of Civil and Mechanical Engineering, Volume 14, Issue 4, 2014. DOI: 10.1016/j.acme.2013.12.005.
17. Y. Liu, Y. Deng, M. Fang, D. Li., D. Wu, Research on the torque characteristics of a seawater hydraulic axial piston motor in deep-sea environment. Ocean Engineering, Volume 146, 2017. DOI: 10.1016/j.oceaneng.2017.10.004.
18. V. Sahoo, D. Roy and R. Maiti, Analysis of Leakage Flow Through the Flank Contacts in Transition Zone in Involute External Toothed Gear Pump. ASME/BATH 2017 Symposium on Fluid Power and Motion Control, Paper No. FPMC2017-4287. DOI: 10.1115/FPMC2017-4287.
19. P. Osinski, A. Deptula, M. Partyka, Discrete optimization of a gear pump after tooth root undercutting by means of multi-valued logic trees, Archives of Civil and Mechanical Engineering 4 (13) (2013), https://doi.org/10.1016/j.acme.2013.05.001.
20. T. Zloto, Simulation of the hydrostatic load of the valve plate-cylinder block system in an axial piston pump. Procedia Engineering, Volume 177, 2017. DOI: 10.1016/j.proeng.2017.02.196.
21. T. Zloto, A. Nagorka, An efficient FEM for pressure analysis of oil film in a piston pump, Applied Mathematics and Mechanics 1 (30) (2009), https://doi.org/10.1007/s10483-009-0106.
22. M. Stosiak, The modeling of hydraulic distributor slide–sleeve interaction. Archives of Civil and Mechanical Engineering 2 (12) (2012), https://doi.org/10.1016/j.acme.2012.04.002.
23. R. Jasinski, Problems of the starting and operating of hydraulic components and systems in low ambient temperature (Part V). Methods Ensuring Correct Start-Up of Hydraulic Components of Ship's Onboard Devices in Low Ambient Temperatures, Polish Maritime Research 4 (96) (2017), https://doi.org/10.1515/pomr-2017-0135.
24. R. Jasinski, Problems of the starting and operating of hydraulic components and systems in low ambient temperature (Part IV). Modelling the heating process and determining the serviceability of hydraulic components during the starting-up in low ambient temperature, Polish Maritime Research 3 (95) (2017), https://doi.org/10.1515/pomr-2017-0089.
25. S. Bednarczyk, Ph.D. thesis: Volumetric losses in orbital pump and the vay of limiting them, Wroclaw University of Technology, 1999.
26. P. Sliwinski, The basics of design and experimental tests of the commutation unit of a hydraulic satellite motor, Archives of Civil and Mechanical Engineering, 4 (16) (2016). https://doi.org/10.1016/j.acme.2016.04.003.
27. P. Sliwinski, Flow of liquid in flat gaps of satellite motors working mechanism, Polish Maritime Research 2 (82) (2014), https://doi.org/10.2478/pomr-2014-0019.
28. P. Sliwinski, The influence of water and mineral oil on volumetric losses in hydraulic motor. Polish Maritime Research S1 (93) (2017), https://doi.org/10.1515/pomr-2017-0041.
29. P. Sliwinski, Research on compensation and valve plate in SM satellite pumps and motors type SM, Hydraulika i Pneumatyka 5 (2010).
30. P. Sliwinski, P. Patrosz, European patent application 15003680.4/EP15003680, Hydraulic Positive Displacement Machine, 29.12.2015.

31. P. Sliwinski, P. Patrosz, Substantive report on the implementation of the contract: „Conducting research in the field of innovative satellite motors with reverse kinematics" for FAMA Ltd. Company in Gniew, Gdansk University of Technology, 2015.
32. P. Sliwinski, Satellite displacement machines. Basic of design and analysis of power loss, Gdansk University of Technology Publishers, 2016.
33. P. Sliwinski, P. Patrosz, Patent PL218888, Satellite operating mechanism of the hydraulic displacement machine, 27.02.2015.